Geoscience Frontiers 9 (2018) 997–1007

HOSTED BY

Contents lists available at ScienceDirect

China University of Geosciences (Beijing)

Geoscience Frontiers

journal homepage: www.elsevier.com/locate/gsf

Research Paper

The dominant driving force for supercontinent breakup: Plume push or subduction retreat?

Nan Zhang [a,b], Zhuo Dang [a], Chuan Huang [a,*], Zheng-Xiang Li [b]

[a] Key Laboratory of Orogenic Belts and Crustal Evolution, School of Earth and Space Sciences, Peking University, Beijing 100871, China
[b] Earth Dynamics Research Group, ARC Center of Excellence for Core to Crust Fluid Systems (CCFS) and The Institute for Geoscience Research (TIGeR), School of Earth and Planetary Sciences, Curtin University, GPO Box U1987, Perth, WA 6845, Australia

ARTICLE INFO

Article history:
Received 1 October 2017
Received in revised form
8 January 2018
Accepted 17 January 2018
Available online 21 February 2018

Keywords:
Supercontinent breakup
Plume push
Subduction retreat

ABSTRACT

Understanding the dominant force responsible for supercontinent breakup is crucial for establishing Earth's geodynamic evolution that includes supercontinent cycles and plate tectonics. Conventionally, two forces have been considered: the push by mantle plumes from the sub-continental mantle which is called the active force for breakup, and the dragging force from oceanic subduction retreat which is called the passive force for breakup. However, the relative importance of these two forces is unclear. Here we model the supercontinent breakup coupled with global mantle convection in order to address this question. Our global model features a spherical harmonic degree-2 structure, which includes a major subduction girdle and two large upwelling (superplume) systems. Based on this global mantle structure, we examine the distribution of extensional stress applied to the supercontinent by both sub-supercontinent mantle upwellings and subduction retreat at the supercontinent peripheral. Our results show that: (1) at the center half of the supercontinent, plume push stress is ~3 times larger than the stress induced by subduction retreat; (2) an average hot anomaly of no higher than 50 K beneath the supercontinent can produce a push force strong enough to cause the initialization of supercontinent breakup; (3) the extensional stress induced by subduction retreat concentrates on a ~600 km wide zone on the boundary of the supercontinent, but has far less impact to the interior of the supercontinent. We therefore conclude that although circum-supercontinent subduction retreat assists supercontinent breakup, sub-supercontinent mantle upwelling is the essential force.

1. Introduction

Supercontinent breakup is a fundamental process of global tectonic evolution, and a key component of both Wilson cycles (Wilson, 1966) and supercontinent cycles (Bleeker, 2003; Rogers and Santosh, 2003; Zhong et al., 2007; Li et al., 2008; Bradley, 2011; Yoshida and Santosh, 2011). Supercontinent breakup has commonly been attributed to either the push power of uprising sub-continental mantle plumes or superplume, or the drag force of retreating slabs (Li et al., 1999; Buiter and Torsvik, 2014; Koptev et al., 2015; Dal Zilio et al., 2017). The former is consistent with the observation that the breakup of Pangea was concurrent with the formation of large igneous provinces (Storey, 1995; Li and Zhong, 2009). The latter was proposed because every supercontinent exhibited abundant subduction records at its boundary (therefore named subduction girdle in Collins, 2003 and Zhong et al., 2007), and the ocean-ward retreat of such a subduction girdle is believed to generate an extensional force that can pull the supercontinent apart (e.g., Bercovici and Long, 2014). Some other studies also suggested gravitational potential force due to sub-continental superswell of mantle plumes or superplume as a force for supercontinent breakup (e.g., Li, 2014) (Fig. 1).

The relevant importance of the various forces in supercontinent breakup has been unclear. Conventionally, plume push from the sub-continental mantle is called the active force for the breakup; whereas the dragging force from the subduction retreat is called the passive force (Fig. 1). The active vs. passive force for the breakup has been intensively debated (e.g., Buiter and Torsvik, 2014; Dal Zilio et al., 2017; Wolstencroft and Davies, 2017), and our study tries to address this question using global 3D modelling.

* Corresponding author.
E-mail address: hchuan@mail.ustc.edu.cn (C. Huang).
Peer-review under responsibility of China University of Geosciences (Beijing).

https://doi.org/10.1016/j.gsf.2018.01.010

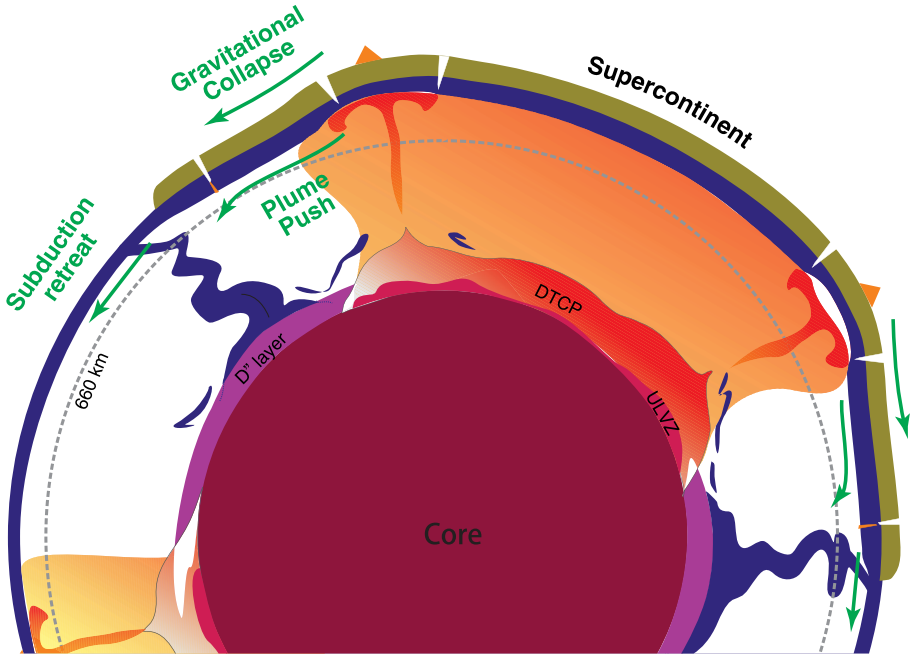

Figure 1. A cartoon demonstrating the three potential forces (including plume push, subduction retreat and gravitational collapse) for supercontinent breakup (after Li, 2014). ULVZ and DTCP are abbreviations for ultra low velocity zones and dense thermo-chemical piles, respectively.

Previous studies of supercontinent and global mantle dynamics (Zhong et al., 2007; Yoshida, 2008; Li and Zhong, 2009; Zhang et al., 2009, 2010; Rolf and Tackley, 2011; Rolf et al., 2012; Yoshida, 2014, 2016) established a good framework for investigating the force balance during supercontinent breakup. The dynamic effects of continental suture zones, rheology and strength have been carefully investigated in Rolf and Tackley (2011), Rolf et al. (2012), and Yoshida (2014). These studies emphasized the importance of continental size, yield stress, or a weak zone within a supercontinent in destabilizing the supercontinent. The series of studies on the long wavelength mantle convection by Zhong et al. (2007), Li and Zhong (2009), and Zhang et al. (2009) have demonstrated a mechanism for supercontinent formation and the influence of a supercontinent on the mantle structure. They predicted that a supercontinent should break up after the formation of a sub-continental superplume (Zhong et al., 2007; Li et al., 2008; Li and Zhong, 2009). The modeled degree-2 mantle structure, featuring a superplume under the supercontinent and an inherited antipodal superswell mimics the present-day mantle structure (Zhong et al., 2007).

Several recent works have also explored the stress caused by subduction retreat (Bercovici and Long, 2014; Holt et al., 2015; Dal Zilio et al., 2017; Yoshida, 2017). All these studies showed that the continental lithosphere (the overriding plate) have an elongated extensional region close to the retreating trench. The horizontal normal stress field along the spherical surface of the overriding plate shows extensional polarity for ~1000 km, from the trench towards the interior of the overriding plate (Holt et al., 2015; Yoshida, 2017). The traction at the bottom of the overriding plate shows a divergent distribution, and after the overriding continental plate breaks completely, the traction in the trench-ward side of the overriding plate would increase (Dal Zilio et al., 2017). However, in these models, another important component for the breakup, i.e., the plumes, is absent. Hence, the fundamental question of which force is more important for the breakup of a supercontinent remains unanswered.

In this work we first build a supercontinent model with global mantle interaction (Zhong et al., 2007; Zhang et al., 2009). Our model shows a plume cluster under the supercontinent, which is self-consistently generated by a circum-supercontinent subduction girdle (Zhong et al., 2007). We use such a mantle structure to quantify the relevant importance of the two driving forces so to address the fundamental question above.

We use numerical mantle convection models with 3D-spherical shell geometry to analyze the spatial variation of extensional stress from the center of the supercontinent to its edge where the subduction occurs. The paper is arranged as follows: section two describes how we setup the models including the model formulations and the mathematical way for calculating the extensional stress, section three presents the model results, and these are followed by the discussion and conclusion sections.

2. Numerical model setup

2.1. Model set-up

We use the model setup of Zhong et al. (2007) and Zhang et al. (2009) as our starting point. Our dynamic models of mantle convection with continental blocks in a three-dimensional spherical geometry assume an infinite Prandtl number and the Boussinesq approximation. The supercontinent block is modeled as a chemically distinct material with different density and viscosity. The non-dimensional governing equations for mantle convection with different compositions (e.g., Zhong et al., 2000; McNamara and Zhong, 2004) are:

$$\nabla \cdot \mathbf{u} = 0 \tag{1}$$

$$-\nabla P + \nabla(\eta \dot{\varepsilon}) = (Ra\delta T - RbC)\mathbf{g} \tag{2}$$

$$\frac{\partial T}{\partial t} + \mathbf{u} \cdot \nabla T = \nabla^2 T + H \tag{3}$$

$$\frac{\partial C}{\partial t} + \mathbf{u} \cdot \nabla C = 0 \tag{4}$$

where **u** is the velocity vector, P is the dynamic pressure, η is the viscosity, $\dot{\varepsilon}$ is the strain rate tensor, δT is the temperature perturbation, **g** is the gravitational acceleration vector, T is the temperature, t is the time, H is internal heat generation rate, and C is the composition using to define continental blocks.

Ra and *Rb,* the Rayleigh number and the chemical Rayleigh number, respectively, are defined as

$$Ra = \alpha\rho g\Delta T R^3 \Big/ (\eta_r \kappa) \tag{5}$$

and

$$Rb = g\delta\rho R^3 \Big/ (\eta_r \kappa) \tag{6}$$

where α is the thermal expansivity, ρ is the density, g is the gravitational acceleration, ΔT is the temperature difference between top and bottom boundaries, R is the radius of the Earth, η_r is the reference viscosity, κ is the thermal diffusivity, and $\delta\rho$ is the density contrast between continents and their surroundings (Table 1). A useful parameter is the buoyancy ratio B defined as

$$B = Rb/Ra = \delta\rho/(\alpha\rho\Delta T) \tag{7}$$

The non-dimensional depth-, temperature-, and composition-dependent viscosity is

$$\eta(r,T,C) = \eta_0(r)\eta_c(C)\exp[E(0.5-T)] \tag{8}$$

where r is the non-dimensional radius, η_0 is the depth dependent prefactor, η_c is the compositional prefactor, and E is the activation energy. The other rheological parameter used is the plasticity, which is controlled by the yield stress. Basically, if the convective stress exceeds the yield stress, the viscosity is reduced to the yielding viscosity

$$\eta_Y = \frac{\sigma_Y}{2\dot{\varepsilon}_{II}} \tag{9}$$

where σ_Y and $\dot{\varepsilon}_{II}$ are the yield stress and the second invariant of strain-rate tensor, respectively. The effective viscosity is then given by $\eta_e = (1/\eta + 1/\eta_Y)^{-1}$. This plasticity formulation is commonly used in previous studies (e.g., Tackley, 2000; Foley and Becker, 2009; Rolf et al., 2012; Yoshida, 2014).

We give an internal heat generation rate of $H = 120$ to yield a 65–70% internal heating (Leng and Zhong, 2009). The thermal Rayleigh number *Ra* in our models is set to 1.5×10^8 (i.e., $Ra = 1.37 \times 10^7$ if the mantle thickness is used to define *Ra*), which gives rise to an average horizontal motion speed of ~5 cm/yr.

The non-dimensional radii for the top and bottom boundaries are 1 and 0.55, respectively. Free-slip and isothermal boundary conditions are applied at the surface and the core-mantle boundary in all calculations. Therefore, the supercontinent is free to move and deform to interact with mantle flows (e.g., Yoshida and Santosh, 2017). The governing equations are solved with code CitcomS (Zhong et al., 2008). Thermochemical convection capability is implemented with the ratio tracer method (Tackley and King, 2003; McNamara and Zhong, 2004) in CitcomS. The mantle is divided into 12 caps and each cap is further divided into 48 elements in three directions. Previous work demonstrated that such a resolution is adequate for this type of calculation (Zhong et al., 2007; Zhang et al., 2009).

The non-dimensional activation energy E in Eq. (8) is set to 6.907 to produce a temperature-induced viscosity variation of 10^3, which allows the mantle convection to remain in the mobile-lid regime (e.g., Solomatov, 1995). Although the activation energy is smaller than that from laboratory studies on olivine, it is used here for numerical stability as well as to account for other weakening effects such as brittle deformation and non-Newtonian rheology. With such an activation energy level and a weak zone to generate the subduction girdle (to be described later), our model can reproduce plate-like behaviors as well as the essential mantle structure. The depth-dependent viscosity prefactor $\eta_0(r)$ is reduced to $\eta_0(r) = 1/30$ for the upper mantle of between 100 km and 670 km depths, and fixed at 1 elsewhere. Such a viscosity profile prefers a long-wavelength planform of mantle convection (Zhong et al., 2007). The initial state of it is shown as the black curve in Fig. 2d.

Compositional prefactor η_c and buoyancy ratio B are used to describe the supercontinent block. Recent work by Watts et al. (2013) showed that continental cratons are much colder and hence much viscous than the oceanic lithosphere. Because a too high η_c may introduce numerical convergence difficulties (Zhang et al., 2009), we set the η_c to 100, which is consistent with previous work (Zhang et al., 2009; Rolf and Tackley, 2011; Yoshida, 2014). B in our models is set at −0.2, which corresponds to a −50 kg/m^3 density contrast between continental lithosphere and oceanic lithosphere. This number is the lower bound for the chemical buoyancy (Jordan, 1978; Poudjom Djomani et al., 2001), which is also used in Rolf et al. (2012). Finally, the supercontinent is modeled as a buoyant and high-viscosity disc that is 200 km thick (e.g., Gung et al., 2003) and occupies 30% of the Earth's surface area.

A 300 km-wide weak zone surrounding the supercontinent is prescribed to facilitate the circum-supercontinent subduction (Gurnis, 1988; Zhong and Gurnis, 1993; Zhong et al., 2007). The viscosity of the weak subduction girdle is reduced by one order (Gurnis, 1989; King and Hager, 1990; Zhong et al., 2007; Dal Zilio et al., 2017) or two orders (Holt et al., 2015) of magnitude relative to the surface oceanic mantle (hence named the ratio of η_g/η_{om}).

Table 1
Model parameters and material properties.

Parameters	Symbols	Value
Density	ρ	3400 kg/m^3
Earth's radius	R	6370 km
Extra density of continents	$\delta\rho$	−50 kg/m^3
Gravitational acceleration	g	10.0 m/s^2
Internal heating rate	H	120
Mantle thickness	d	2870 km
Temperature difference	ΔT	2800 K
Thermal diffusivity	κ	10^{-6} m^2/s
Thermal expansion	α	3×10^{-5} K^{-1}
Rayleigh number	*Ra*	1.5×10^8
Reference viscosity	η_r	5×10^{21} Pa·s
Specific heat	C_p	1200 J/(kg·K)

2.2. Modeling parameters and initial conditions

Our models involve three important parameters: the yield stress of continents, the viscosity of subduction weak zone, and the trench retreat rate (Table 2). These parameters have direct influences on the forces of supercontinent breakup although the first two are related. The prescribed weak zone in the oceanic lithosphere surrounding the supercontinent is a simple way to implement the plastic yielding for the subduction system surrounding the supercontinent. With such a simplification for the subduction girdle, we are able to obtain Earth-like plate tectonics, and uncouple the oceanic lithosphere from the continental lithosphere because the oceanic lithosphere is separated from the supercontinent by the subduction girdle. A selective application of the yielding stress to the continental side only allows us to focus on the stress distribution within the supercontinent. Neglecting the localized yielding in the oceanic lithosphere also leads to a faster computational convergence.

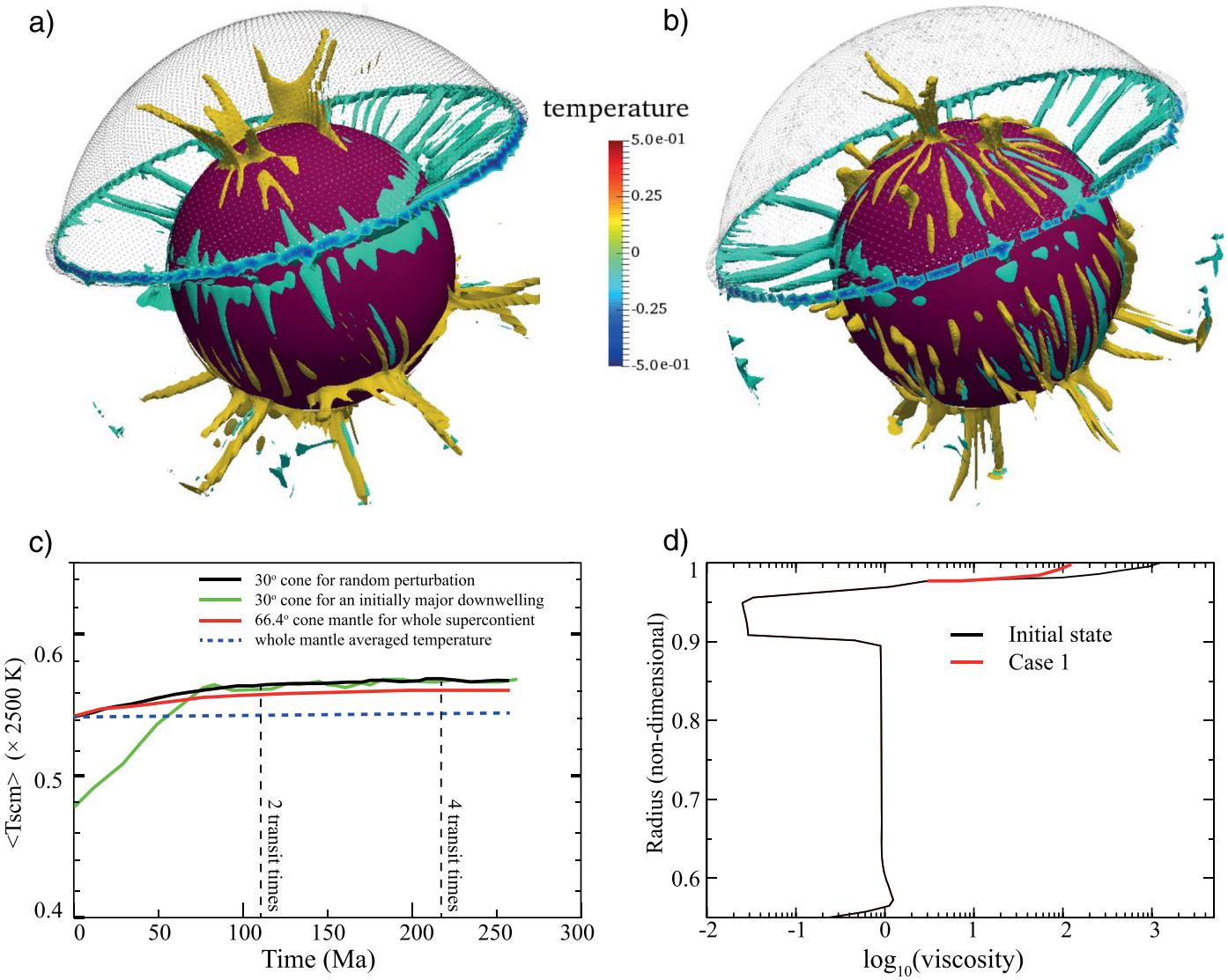

Figure 2. Preparation of initial modeling condition. The supercontinent (transparent gray) covers 30% of Earth's surface area. A subduction girdle with low viscosity is imposed at the edge to generate the planform-two upwelling system (Zhong et al., 2007), of which mantle structures after 2 transit time (a) and 4 transit time (b) are shown. The comparison of average temperatures beneath the supercontinent and that of the whole mantle are presented in (c). (d) shows the azimuthally averaged viscosity profiles.

Different from Rolf et al. (2012) and Yoshida (2014), the yield stresses (50 or 100 MPa) in the continental area of our models are 2–4 times smaller than that for the oceanic lithosphere, which is derived from the mean strength ratio of oceanic to continental lithosphere (~3.3) based on Kohlstedt et al. (1995) results (see Fig. 9 of Kohlstedt et al., 1995). Experimental results (e.g., Goetze and Poirier, 1978; Brace and Kohlstedt, 1980; Kohlstedt et al., 1995) show that the yielding strength for felsic rocks is lower than that for mafic rocks. The reason behind is that felsic rocks are more sensitive to high temperature in the lithosphere (Kohlstedt et al., 1995).

The viscosity for the weak zone (hence the ratio η_g/η_{om}) determines the strength of the return flow in the mantle wedge (Yoshida, 2017) as well as the extensional stress on the top of the return flow. We will use η_g/η_{om} values of 0.1 and 0.01 in our models.

The rate for trench retreat has a large range of 0.1 cm/yr (Schellart et al., 2008) to 3 cm/yr (the Western Pacific). We manually force the subduction girdle to retreat, although the causes for the retreat are still debated (e.g., Holt et al., 2015; Yoshida, 2017). Such a large range of retreat rates can potentially cause different extensional stresses on the overriding continental lithosphere. Two retreating rates of 0.5 cm/yr and 2 cm/yr were used in our simulations.

To prepare reasonable initial hot upwellings beneath the supercontinent before its breakup, we perform two-step calculations

Table 2
The model settings.

Case No.	Retreat rate (cm/yr)	Weak zone viscosity ratio (i.e. η_g/η_{om})	Yield stress (MPa)
1[a] (I, II, and III)	2	0.1	50
2 (I, II, and III)	2	0.01	50
3 (I, II, and III)	2	0.1	100
4 (I, II, and III)	2	0.01	100
5 (I, II, and III)	0.5	0.1	50
6 (I, II, and III)	0.5	0.1	100

[a] Every case has three different runs. The first (I) includes both the hot plumes and the subduction girdle; the second (II) has the subduction girdle removed but keeps the hot plume structures; and the third (III) has the hot plumes removed but keeps the subduction girdle.

based on experiences from previous models (Zhong et al., 2007; Zhang et al., 2009) as well as geological constraints. In the first step, a pure thermal convection model is computed for a given set of parameters until global average quantities (e.g., heat flux and root-mean-square velocity) reach a statistical steady-state. In the second step, for the same model parameters, using the steady-state temperature field profile from the purely thermal convection model as the initial temperature condition, a supercontinent block and a peripheral subduction girdle (low viscosity zone) are introduced to examine the sub-continental upwelling generation. During the second step, the subduction girdle will not retreat and the continental yield stress is not yet applicable to the supercontinent. This second step of model set-up assumes that the supercontinent has just been assembled and it will remain stable until its breakup starts. We run the model for 4 transit times (the transit time depicts the time-span of a particle travels from the top to the bottom of the mantle, which is set to ~55 Myr in this work, corresponding a traveling velocity of 5.2 cm/yr) to prepare appropriate sub-continental upwellings for supercontinent breakup because the lifetimes for supercontinents Pangea (Scotese, 2001), Rodinia (Li and Evans, 2011), and Nuna (Pisarevsky et al., 2014) are all around 150–200 Myr (also see discussion in Li and Zhong, 2009).

With the subduction girdle and supercontinent in place, a global spherical harmonic degree-2 structure, including a cluster of hot upwellings beneath the supercontinent (Fig. 2a and b) is generated after ~1 transit time. During the first transit time, the average sub-continental mantle temperature over the region with an arc radian of 30° from the center of the supercontinent, T_{scm}, increases faster than afterwards (black curve in Fig. 2c). We also run a test with an initial major downwelling beneath the supercontinent as in Zhong et al. (2007) (green curve in Fig. 2c), but T_{scm} does not show much difference after 1.5 transit time. The positive temperature anomaly under the supercontinent is ~50 K above the average mantle temperature after it reaches relatively stable at 1 transit time (the red and blue curves in Fig. 2c). This temperature difference is similar to that of Yoshida (2014), but smaller than that of >100 K as in Rolf et al. (2012). We think that the higher temperature difference of Rolf et al. (2012) is caused by both their pure internal heating model and the far smaller Rayleigh number they used.

After four transit times of convection and a reasonable generation of hot upwellings under the supercontinent, we introduce the yield stress for the supercontinent and a retreat velocity of subduction girdle. The latter is achieved through by manually relocating the low viscosity zone for every computation step. With this implementation, a subduction rate of ~6.5 cm/yr is observed along the subduction girdle.

2.3. Calculation of extensional stress

The CitcomS mantle convection code was built based on spherical coordinates (Zhong et al., 2008). Hence, the calculated global deviatoric stress field is also spherical coordinates-based. We use Cauchy stress transformation (Taylor, 2005) to calculate the extensional stress along the great-circle between the center of a supercontinent and its edge (e.g., $\overset{\frown}{CE}$ in Fig. 3). To ensure the reliability of our results, the extensional stress on three equal-spaced transects (green lines in Fig. 3) are calculated. Our final results will be the average of the stress values along the three transects.

For any point P and given stress tensor $\boldsymbol{\sigma}_p$ (the difference of viscous stress and dynamic pressure) at that point, the normal component of the stress on the plane perpendicular to $\overset{\frown}{CE}$ is the extensional stress, which can be calculated as:

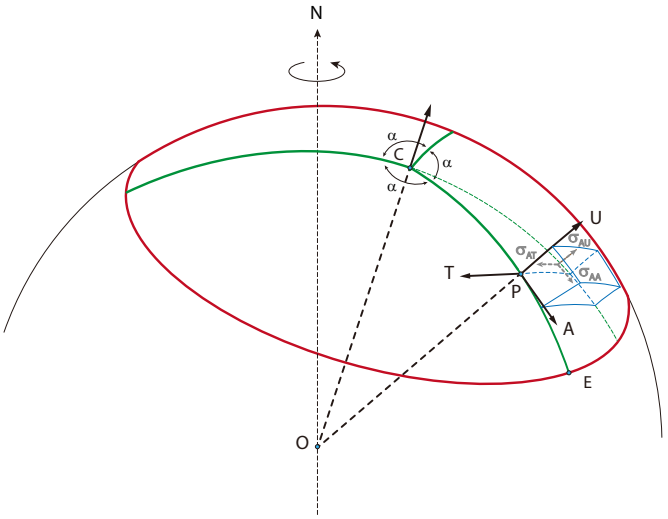

Figure 3. The geometry and vector map used for calculating the extensional stress σ_{AA} from the center (C) to the edge (E) of a supercontinent (area surrounded by red curves). The final tensile stress will be the average for the three transects marked by green solid lines on the map. $\overrightarrow{PA}$ denotes the tangential direction of the arc $\overset{\frown}{CE}$ at point P. Vector $\overrightarrow{PT}$ is perpendicular to the surface determined by points C, P and O. $\overrightarrow{PU}$ follows the direction determined by line OP.

$$\sigma_{AA} = \boldsymbol{\sigma}_p \cdot \frac{\overrightarrow{PA}}{|\overrightarrow{PA}|} \cdot \frac{\overrightarrow{PA}}{|\overrightarrow{PA}|} \tag{10}$$

where σ_{AA} is the extensional stress, $\overrightarrow{PA}$ is the vector tangential to $\overset{\frown}{CE}$ at point P (Fig. 3). As shown in Fig. 3, the vector $\overrightarrow{PA}$ can be expressed as the cross product of $\overrightarrow{PU}$ and $\overrightarrow{PT}$, where $\overrightarrow{PT}$ is the cross product of $\overrightarrow{OP}$ and $\overrightarrow{OC}$. We use an extra tracer flavor to track the supercontinent center C, and find that our supercontinent center moves less than 1° from its initial location within one transit time.

3. Results

We conducted six cases by varying three parameters: yield stress, weak zone viscosity ratio, and subduction retreat rate (Table 2). We identify the supercontinent breakup when the continental middle depth of 100 km is penetrated by hotter mantle material (e.g., Fig. 4c). To see clearly the plume push effect vs. the effect of subduction retreat, we carried out three stokes solutions with (1) both structures of hot anomalies beneath the supercontinent and the cold subduction girdle, (2) only the hot anomaly structures, and (3) only the cold subduction girdle, for the output stress tensor $\boldsymbol{\sigma}_p$ of a particular step. The division between hot anomalies beneath the supercontinent and the cold girdle at the supercontinent peripheral is conducted by an arc with a 50° radian from the center of the supercontinent (the white sector in Fig. 4b). The areas from the supercontinent center to the edge of the arc, and from the edge of the arc to the girdle, represent the main regions that plume and slab subduction occurs, respectively. This operation is not a pure linear system, and will be further discussed in Section 4. We calculated and plotted the extensional stress σ_{AA} as in Fig. 5.

We demonstrate our modeling results starting from standard Case 1 (Table 2) which has a continental yield stress of 50 MPa, a subduction retreat rate of 2.0 cm/yr, and a η_g/η_{om} ratio of 0.1. The application of 50 MPa continental yield stress reduces the average effective surface viscosity (red curve in Fig. 2d). After ~21 Myr, the plume heads have caused patchy areas of weakening at the

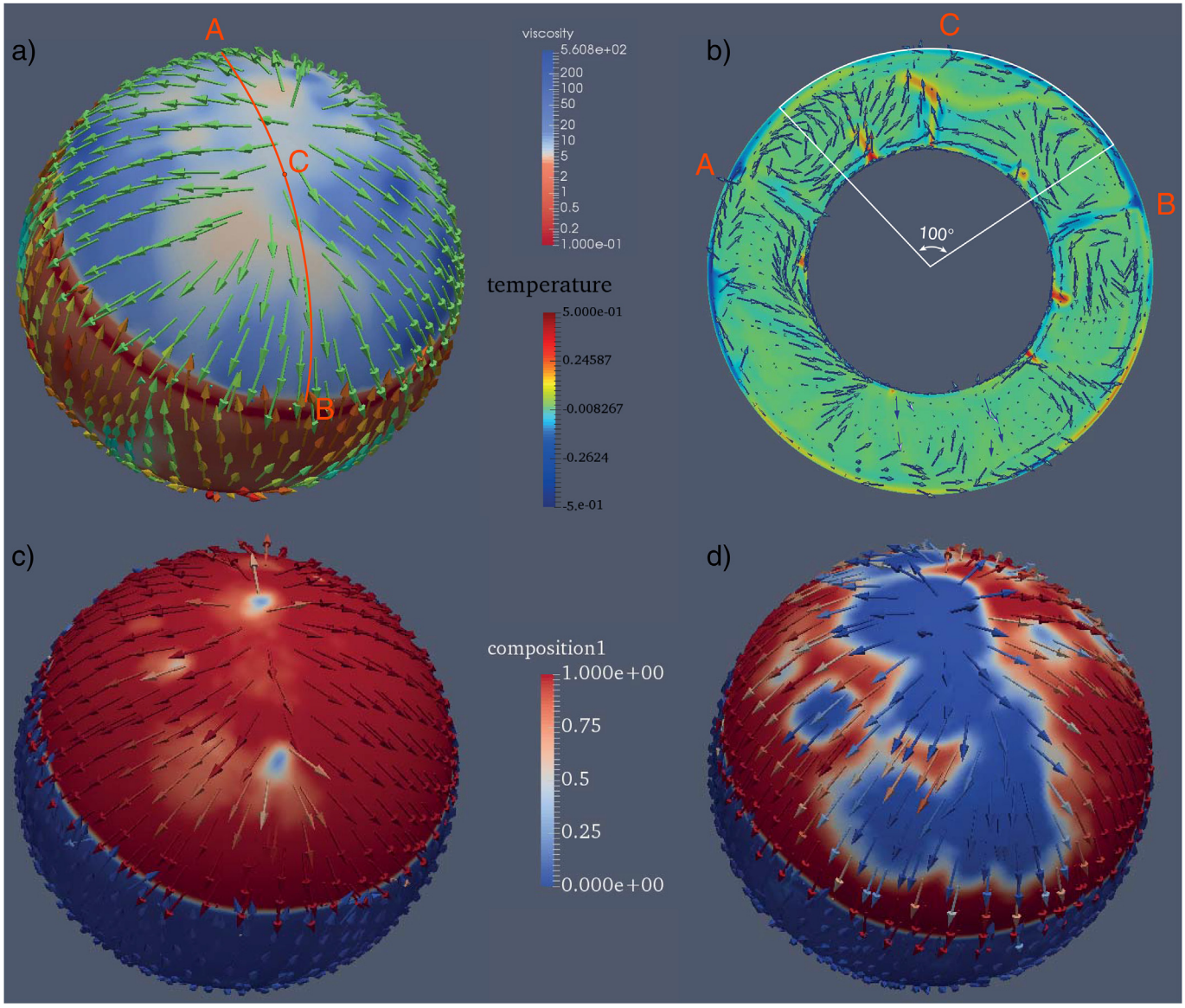

Figure 4. The various fields of Case 1 during and after the supercontinent breakup. The viscosity and flow velocity at the depth of 75 km at model time of 21 Myr are shown in (a). For the same model time, the temperature and velocity in the cross-section along the great-circle A–C–B (b), and composition field at the depth of 100 km (c), are shown. After 65 Myr of model time, the composition field is shown in (d).

lithosphere (Fig. 4a) and led to hot mantle material penetrating to 100 km depth (Fig. 4c). The mantle shows strong upwellings above the plume cluster and return flows in the mantle wedge under the overriding supercontinent (Fig. 4b). The distribution of weakened areas is certainly not symmetric. After 65 Myr, the supercontinent starts to tear apart from inside to many pieces (Fig. 4d). The shapes of the continental blocks are understandably different from the present-day continental margins because we have not taken into account the effect of preexisting weak zones (e.g., Buiter and Torsvik, 2014; Yoshida, 2014; Yoshida and Hamano, 2015). This effect will be further discussed in Section 4.

The average extensional stresses σ_{AA} from three stokes solutions, at 21 Myr of model calculation, are presented in Fig. 5. We show them at the depths of 75 km and 220 km, which represent the stress state at the middle of the continental lithosphere and at the top of the asthenosphere, respectively. The extensional stress caused by both hot plumes and cold slabs shows a positive high of ~40 MPa at the central area which gradually decreases to zero ~600 km before reaching the edge (Fig. 5a). When approaching the trench, there is a rise in extensional stress to ~15 MPa due to the return flow in the mantle wedge (Fig. 4b). When we manually remove the subduction girdle and hence the down wellings at the supercontinent peripheral (Fig. 6a), the extensional stress still reaches ~35 MPa at the central area and has a trend similar to the model result containing both hot and cold structures, except for the 600 km belt along the trench (Fig. 5b). On the other hand, in the stokes solution without hot anomalies beneath the supercontinent (Fig. 6b) but return flows in the mantle wedges, the extensional stress is ~5 MPa at the central area of the supercontinent and reaches ~15 MPa at its edge (Fig. 5c). This stress distribution compensates that with only hot anomalies, especially at the 600 km-wide zone close to the trench. A comparison between Fig. 5b and c shows that the plume push stress is ~3 times stronger than the stress induced by subduction retreat in the central region

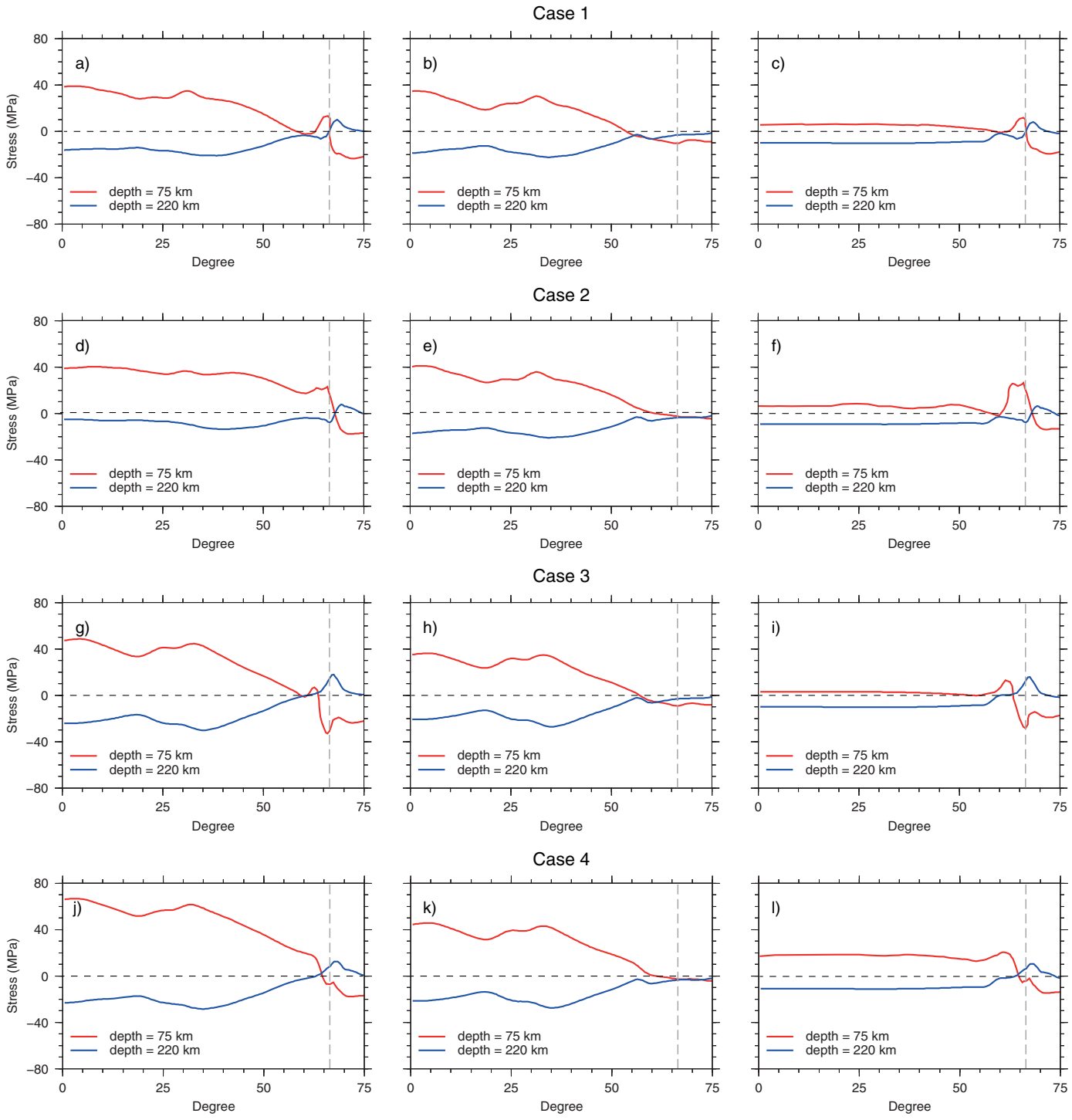

Figure 5. The average extensional stress distributions for Case 1 (a–c), Case 2 (d–f), Case 3 (g–i) and Case 4 (j–l) at 21 Myr of model time. The left panel shows the results including both the effects of subduction girdle and hot plumes beneath the supercontinent. In the middle panel, the influences of girdle are removed while the effects of hot plumes are kept. In the right panel, we removed the hot plumes but kept the girdle structure. The horizontal axes denote the distance (measured in degree) of a point from the center of the supercontinent, where the gray dash line shows the position where the edge of the supercontinent locates. In each plot, the positive values mean extension, while negative values denote compression. The stresses at the depths of 75 km and 220 km are plotted in red and blue lines, respectively.

of the supercontinent. The stress due to subduction retreat mostly affects the area within ~600 km from the trench, but has little influence to the interior of the supercontinent.

The effect of a different η_g/η_{om} value of 0.01 is shown in Case 2 (Table 2 and Fig. 5d–f). A weaker mantle wedge leads to a stronger return flow beneath the overriding supercontinent, and the major difference occurs at the area close to the trench. The extensional stress induced by the return flow becomes ~2 times larger (Fig. 5f vs. 5c), while the plume push stress maintains its previous level (Fig. 5e vs. 5b).

Next, the effect of a stronger continental yield stress on the extensional stresses is demonstrated in Case 3 and Case 4, which are the same as Case 1 and Case 2 respectively, except that the yield stress is doubled (i.e. 100 MPa, Table 2). With such an increased yield stress,

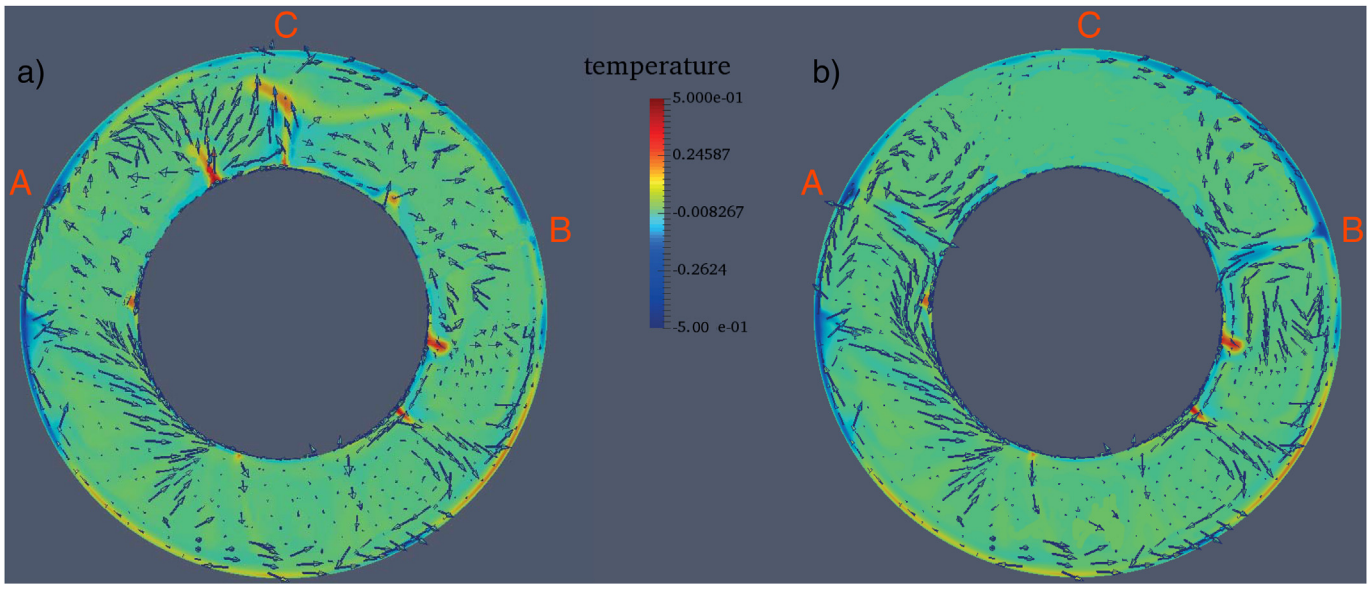

Figure 6. The two stokes solutions along A–C–B cross-section marked in Fig. 4. The stokes flow without the subduction girdle is presented in (a), whereas that without the hot anomalies under the supercontinent is presented in (b).

the extensional stresses at the center of the supercontinent increased to 10–25 MPa (Fig. 5g vs. 5a and Fig. 5j vs. 5d).

We note that models with a slower trench retreat rate of 0.5 cm/yr (Case 5 and Case 6 in Table 2) show insignificant difference from models with a trench retreat rate of 2 cm/yr (Figs. 7a and 5a, and Figs. 7d and 5g). This could be interpreted to reflect the limited effect of trench retreat, but the effects of weak zone width need to be clarified in future work. We also notice the stresses in the asthenosphere beneath the supercontinent show compressional polarities (blue curves in Figs. 5 and 7). This is likely caused by the gathering of return flows beneath the lithosphere.

4. Discussions

Our modeled stress distribution is the first such work that systematically investigated the relative contributions to extensional stress during supercontinent breakup from plume push and subduction retreat. The modeled stress induced by the retreating subduction alone (e.g., Fig. 5c) shows that the highest extensional stress occurs above the subduction zone, but the stress regime then switches to a compressional state before returning to a weakly extensional one toward the interior of the supercontinent. This trend, as well as the magnitude in resultant stress regime, is

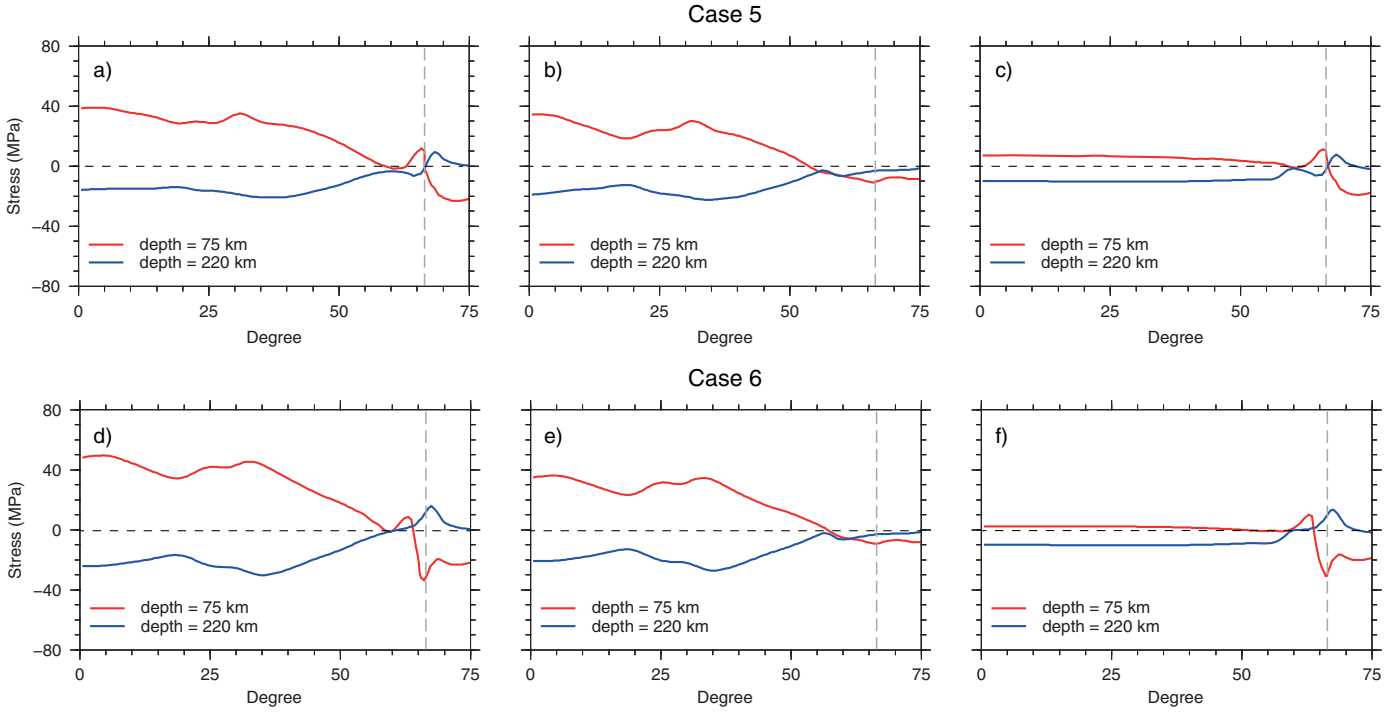

Figure 7. Average extensional stress distributions for cases with only 0.5 cm/yr trench retreat speed. (a–c) are for Case 5, and (d–f) are for Case 6. See the caption of Fig. 5 for details.

generally consistent with the results of Holt et al. (2015). The stress due to the sub-continental plume-push is estimated systematically for the first time here with a plume cluster structure, which is generated predominantly by the global subduction girdle (with relatively minor contribution from supercontinent insulation). This global girdle is well documented in the present-day Earth as a legacy of the Pangea supercontinent cycle, and is speculated to have presented in previous supercontinent cycles as well (Zhong et al., 2007; Li et al., 2008; Li and Zhong, 2009). In the spherical geometry, it is inevitable to generate the hot plume cluster in the supercontinent hemisphere when the subduction girdle forms (Zhong et al., 2007).

The stokes flow is mainly controlled by three mantle thermal structures, i.e., the sub-continental hot plume cluster, the cold subduction girdle, and the major upwelling antipodal to the supercontinent. Hence mathematically, the linear superposition of the stokes solutions without the cold subduction retreat (Fig. 5b) and that without hot plume cluster (Fig. 5c) cannot be perfectly equal to the stokes solution with all the three structures (Fig. 5a). However, in practice, we find that these two solutions generally compensate to each other in the first order (e.g., Fig. 5b and c). This may imply that the antipodal upwelling is too far to have obvious effects on the supercontinent breakup. Hence, the technique used herein to discriminate stress contributions from the hot plume cluster and subduction retreat is reliable on a first-order basis.

Our model has not included any pre-existing weak zones in the supercontinent as in some other studies (Buiter and Torsvik, 2014; Yoshida, 2014; Yoshida and Hamano, 2015). Our work instead focuses on testing theoretical concepts in the first-order, and the results should therefore be considered as theoretical predictions. We predict that subduction retreat alone cannot break up a supercontinent. To further verify this, we tried a tentative calculation, similar to Case 1, but with continuously removing the hot anomalies under the supercontinent at every computation step. Although this kind of calculation is not energy conservative, we could track the trend of stress induced by the subduction retreat. The model evolution is shown in Fig. 8. After 20 Myr of model evolution, the supercontinent is still largely intact (red area in Fig. 8a). The deformation area is mostly localized at regions close to the trench (green zone in Fig. 8a). After ~100 Myr, the stress deforms the supercontinent a little more toward the interior (Fig. 8b). Although one side of the supercontinent is already ruptured along the edge by subduction retreat, the bulk of the interior part of the supercontinent remains intact. A similar result is shown in a modeling work with regional cartesian geometry by Dal Zilio et al. (2017).

Yoshida (2014), on the other hand, suggested that subduction retreat, together with pre-existing weak zones, can pull Pangea apart without any plume from the CMB. In that model, the anomalous mantle temperature beneath the supercontinent is ~50 K higher than that within the non-continental area. However, our models show that, with a <50 K hot anomaly beneath the supercontinent, the push stress can be ~3 times bigger than stress induced by subduction retreat, especially at the center of the supercontinent. This magnitude of plume-induced stress shows its importance, although our models have no pre-existing weak zones, and hence could not identify the exact pattern of supercontinent breakup. The role of plume push has been included as an initial condition in Yoshida and Hamano (2015) to produce the breakup of Pangea. Although the role of plume is not accurately quantified in that study, its flow pattern is consistent with our results.

Our modeled mantle temperature is mainly relevant to the supercontinent events after the Proterozoic. For earlier supercontinent events such as Rodinia and Nuna, the mantle temperature should have been higher because the Earth was much hotter and more convectively vigorous (Condie, 2005). Hence, mantle plume

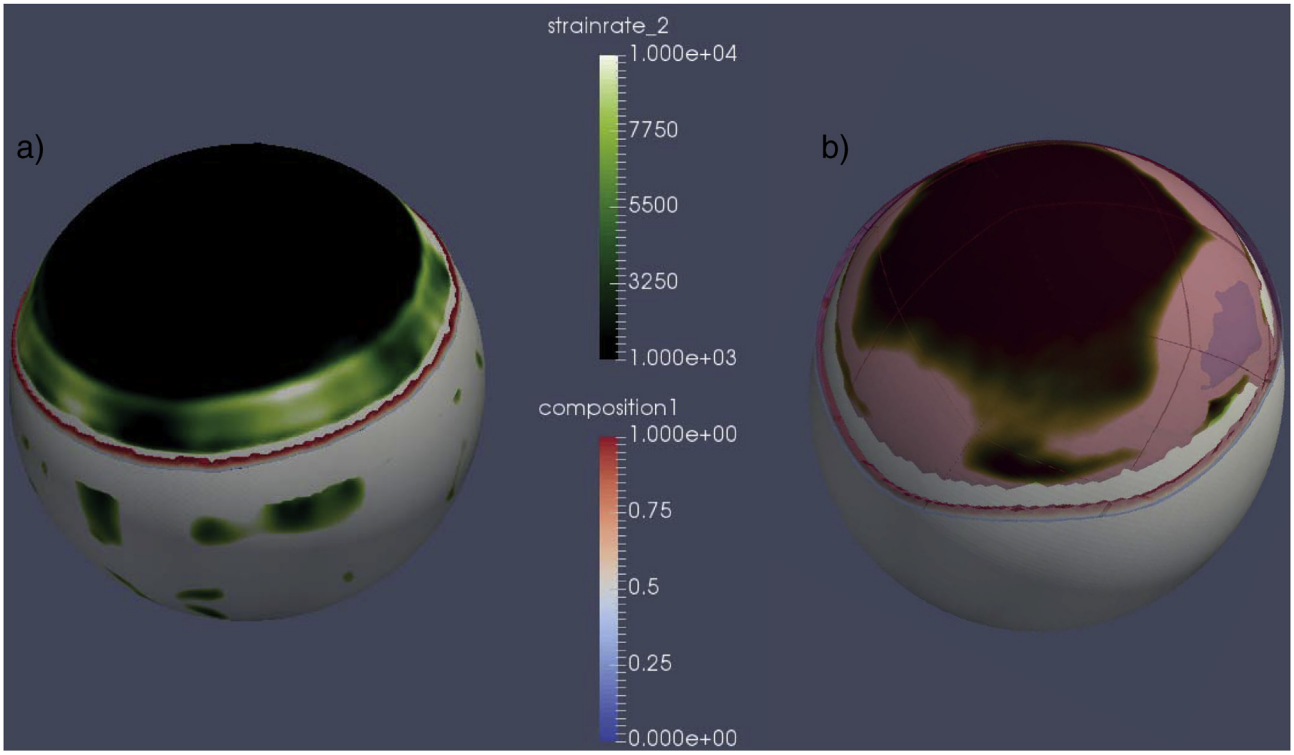

Figure 8. A tentative case exploring the long-term evolution of supercontinent deformation without hot anomalies beneath the supercontinent. This calculation attempts to isolate the role of subduction girdle. The deformation of the supercontinent is presented at 20 Myr (a) and 100 Myr (b) of model time, respectively. The green color represents the second invariant of strain rate, while the transparent red represents the compositional field.

could be playing an even more dominant role in supercontinent breakup then.

Our modeled continental lithosphere thickness is set at 200 km, which is thinner than what the seismic anisotropy data predict (Gung et al., 2003) but is consistent with waveform tomography and xenoliths derived thickness of ~190 km (e.g., French et al., 2013; Tharimena et al., 2017). With a thicker continental lithosphere, the average temperature beneath the supercontinent should be hotter.

Our models have not included the basal traction force beneath the supercontinent (e.g., Yoshida, 2010) because our preliminary results of the basal traction calculation showed a relatively small magnitude compared to the extensional normal stress σ_{AA}. However, future work will include a complete analysis for the supercontinent forces and calculate the balance between the extensional force and the basal traction force.

5. Conclusions

We conclude the followings based on our modeling results:

(1) Plume push stress is ~3 times larger than that induced by subduction retreat within the interior of the supercontinent for its breakup.
(2) An average hot anomaly of no higher than 50 K beneath a supercontinent is sufficient to produce a strong extensional stress to cause the initialization of supercontinent breakup.
(3) The induced extensional stress by subduction retreat concentrates on a 600 km-wide zone close to the trench. For the interior of the supercontinent, the stress generated by subduction retreat is relatively insignificant in comparison with the stress generated by plumes.
(4) The strength of a supercontinent (the yield stress) influences the magnitude of plume-push stress; the viscosity ratio between the weak zone and the mantle (η_g/η_{om}) has the essential effect on the magnitude of the stress induced by subduction retreat.

Acknowledgements

We thank Christopher Spencer for helpful comments on an earlier version of this manuscript. Review comments by Masaki Yoshida and an anonymous reviewer, and comments from editors Richard Palin and M. Santosh, helped to improve the clarity of the manuscript. This work was supported by Australian Research Council Australian Laureate Fellowship grant to ZXL (FL150100133), and by China's Thousand Talents Plan (2015) and NSFC41674098 to NZ. Computational Infrastructure for Geodynamics is thanked for distributing the software CitcomS that is used in this study. Computational work was supported by resources provided by the High-performance Computing Platform of Peking University and the Pawsey Supercomputing Centre with funding from the Australian Government and the Government of Western Australia. This is CCFS contribution 1033, and a contribution to IGCP 648.

References

Bercovici, D., Long, M.D., 2014. Slab rollback instability and supercontinent dispersal. Geophysical Research Letters 41, 6659–6666.
Bleeker, W., 2003. The late archean record: a puzzle in ca. 35 pieces. Lithos 71, 99–134.
Brace, W.F., Kohlstedt, D.L., 1980. Limits on lithospheric stress imposed by laboratory experiments. Journal of Geophysical Research: Solid Earth 85, 6248–6252.
Bradley, D.C., 2011. Secular trends in the geologic record and the supercontinent cycle. Earth-Science Reviews 108, 16–33.
Buiter, S.J.H., Torsvik, T.H., 2014. A review of wilson cycle plate margins: a role for mantle plumes in continental breakup along sutures? Gondwana Research 26, 627–653.
Collins, W.J., 2003. Slab pull, mantle convection, and Pangaean assembly and dispersal. Earth and Planetary Science Letters 205, 225–237.
Condie, K.C., 2005. Earth as an Evolving Planetary System. Academic Press, Burlington, pp. 1–11.
Dal Zilio, L., Faccenda, M., Capitanio, F., 2017. The role of deep subduction in supercontinent breakup. Tectonophysics. https://doi.org/10.1016/j.tecto.2017.03.006.
French, S., Lekic, V., Romanowicz, B., 2013. Waveform tomography reveals channeled flow at the base of the oceanic asthenosphere. Science 342, 227–230.
Foley, B.J., Becker, T.W., 2009. Generation of plate-like behavior and mantle heterogeneity from a spherical, viscoplastic convection model. Geochemistry, Geophysics, Geosystems 10. https://doi.org/10.1029/2009GC002378.
Goetze, C., Poirier, J.P., 1978. The mechanisms of creep in olivine. Philosophical Transactions of the Royal Society of London. Series A: Mathematical, Physical and Engineering Sciences 288, 99–119.
Gung, Y., Panning, M., Romanowicz, B., 2003. Global anisotropy and the thickness of continents. Nature 422, 707–711.
Gurnis, M., 1988. Large-scale mantle convection and the aggregation and dispersal of supercontinents. Nature 332, 695–699.
Gurnis, M., 1989. A reassessment of the heat transport by variable viscosity convection with plates and lids. Geophysical Research Letters 16, 179–182.
Holt, A.F., Becker, T.W., Buffett, B.A., 2015. Trench migration and overriding plate stress in dynamic subduction models. Geophysical Journal International 201, 172–192.
Jordan, T.H., 1978. Composition and development of the continental tectosphere. Nature 274, 544–548.
King, S.D., Hager, B.H., 1990. The relationship between plate velocity and trench viscosity in Newtonian and power-law subduction calculations. Geophysical Research Letters 17, 2409–2412.
Koptev, A., Calais, E., Burov, E., Leroy, S., Gerya, T., 2015. Dual continental rift systems generated by plume-lithosphere interaction. Nature Geoscience 8, 388–392.
Kohlstedt, D.L., Evans, B., Mackwell, S.J., 1995. Strength of the lithosphere: constraints imposed by laboratory experiments. Journal of Geophysical Research: Solid Earth 100, 17587–17602.
Leng, W., Zhong, S., 2009. More constraints on internal heating rate of the earth's mantle from plume observations. Geophysical Research Letters 36. https://doi.org/10.1029/2008GL036449.
Li, Z.X., 2014. Supercontinent break-up: causes and consequences. In: AGU Fall Meeting. San Francisco, CA. T33B–4655.
Li, Z.X., Bogdanova, S.V., Collins, A.S., Davidson, A., De Waele, B., Ernst, R.E., Fitzsimons, I.C.W., Fuck, R.A., Gladkochub, D.P., Jacobs, J., Karlstrom, K.E., Lu, S., Natapov, L.M., Pease, V., Pisarevsky, S.A., Thrane, K., Vernikovsky, V., 2008. Assembly, configuration, and break-up history of Rodinia: a synthesis. Precambrian Research 160, 179–210.
Li, Z.X., Evans, D.A.D., 2011. Late neoproterozoic 40 intraplate rotation within Australia allows for a tighter-fitting and longer-lasting Rodinia. Geology 39, 39–42.
Li, Z.X., Li, X.H., Kinny, P.D., Wang, J., 1999. The breakup of Rodinia: did it start with a mantle plume beneath South China? Earth and Planetary Science Letters 173, 171–181.
Li, Z.X., Zhong, S., 2009. Supercontinent-superplume coupling, true polar wander and plume mobility: plate dominance in whole-mantle tectonics. Physics of the Earth and Planetary Interiors 176, 143–156.
McNamara, A.K., Zhong, S., 2004. Thermochemical structures within a spherical mantle: superplumes or piles? Journal of Geophysical Research: Solid Earth 109. https://doi.org/10.1029/2003JB002847.
Pisarevsky, S.A., Elming, S.Å., Pesonen, L.J., Li, Z.X., 2014. Mesoproterozoic paleogeography: supercontinent and beyond. Precambrian Research 244, 207–225.
Poudjom Djomani, Y.H., O'Reilly, S.Y., Griffin, W.L., Morgan, P., 2001. The density structure of subcontinental lithosphere through time. Earth and Planetary Science Letters 184, 605–621.
Rogers, J.J.W., Santosh, M., 2003. Supercontinents in earth history. Gondwana Research 6, 357–368.
Rolf, T., Coltice, N., Tackley, P., 2012. Linking continental drift, plate tectonics and the thermal state of the earth's mantle. Earth and Planetary Science Letters 351, 134–146.
Rolf, T., Tackley, P.J., 2011. Focussing of stress by continents in 3D spherical mantle convection with self-consistent plate tectonics. Geophysical Research Letters 38, 113–120.
Schellart, W.P., Stegman, D.R., Freeman, J., 2008. Global trench migration velocities and slab migration induced upper mantle volume fluxes: constraints to find an earth reference frame based on minimizing viscous dissipation. Earth-Science Reviews 88, 118–144.
Scotese, C.R., 2001. Atlas of Earth History, 1. Paleogeography, PALEOMAP Project, Arlington, Texas, p. 58.
Solomatov, V.S., 1995. Scaling of temperature- and stress-dependent viscosity convection. Physics of Fluids 7, 266–274.
Storey, B.C., 1995. The role of mantle plumes in continental breakup: case histories from Gondwanaland. Nature 377, 301–308.
Tackley, P.J., 2000. Self-consistent generation of tectonics plates in time-dependent, three-dimensional mantle convection simulations: 1. Pseudoplastic yielding. Geochemistry, Geophysics, Geosystems 1. https://doi.org/10.1029/2000GC000036.

Tackley, P.J., King, S.D., 2003. Testing the tracer ratio method for modeling active compositional fields in mantle convection simulations. Geochemistry, Geophysics, Geosystems 4. https://doi.org/10.1029/2001GC000214.
Taylor, J.R., 2005. Classical Mechanics. University Science Books, Sausalito, CA, p. 786.
Tharimena, S., Rychert, C., Harmon, N., 2017. A unified continental thickness from seismology and diamonds suggests a melt-defined plate. Science 357, 580–583.
Watts, A., Zhong, S.J., Hunter, J., 2013. The behavior of the lithosphere on seismic to geologic timescales. Annual Review of Earth and Planetary Sciences 41, 443–468.
Wilson, J.T., 1966. Did the Atlantic close and then re-open? Nature 211, 676–681.
Wolstencroft, M., Davies, J.H., 2017. Breaking supercontinents; no need to choose between passive or active. Solid Earth 8, 817–825.
Yoshida, M., 2008. Mantle convection with longest-wavelength thermal heterogeneity in a 3-D spherical model: degree one or two? Geophysical Research Letters 35, 186–203.
Yoshida, M., 2010. Temporal evolution of the stress state in a supercontinent during mantle reorganization. Geophysical Journal International 180. https://doi.org/10.1111/j.1365-246X.2009.04399.x.
Yoshida, M., 2014. Effects of various lithospheric yield stresses and different mantle-heating modes on the breakup of the Pangea supercontinent. Geophysical Research Letters 41, 3060–3067.
Yoshida, M., 2016. Formation of a future supercontinent through plate motion-driven flow coupled with mantle downwelling flow. Geology 44, 755–758.
Yoshida, M., 2017. Trench dynamics: effects of dynamically migrating trench on subducting slab morphology and characteristics of subduction zones systems. Physics of the Earth and Planetary Interiors 268, 35–53.
Yoshida, M., Hamano, Y., 2015. Pangea breakup and northward drift of the Indian subcontinent reproduced by a numerical model of mantle convection. Scientific Reports 5. https://doi.org/10.1038/srep08407.
Yoshida, M., Santosh, M., 2011. Supercontinents, mantle dynamics and plate tectonics: a perspective based on conceptual vs. numerical models. Earth-Science Reviews 105. https://doi.org/10.1016/j.earscirev.2010.12.002.
Yoshida, M., Santosh, M., 2017. Voyage of the Indian subcontinent since Pangea breakup and driving force of supercontinent cycles: insights on dynamics from numerical modeling. Geoscience Frontiers (in press).
Zhang, N., Zhong, S., Leng, W., Li, Z.X., 2010. A model for the evolution of the Earth's mantle structure since the Early Paleozoic. Journal of Geophysical Research 115. https://doi.org/10.1029/2009JB006896.
Zhang, N., Zhong, S., McNamara, A.K., 2009. Supercontinent formation from stochastic collision and mantle convection models. Gondwana Research 15, 267–275.
Zhong, S., Gurnis, M., 1993. Dynamic feedback between an continentlike raft and thermal convection. Journal of Geophysical Research 98, 12219–12232.
Zhong, S., McNamara, A., Tan, E., Moresi, L., Gurnis, M., 2008. A benchmark study on mantle convection in a 3-D spherical shell using CitcomS. Geochemistry, Geophysics, Geosystems 9, 806–815.
Zhong, S., Zhang, N., Li, Z.X., Roberts, J.H., 2007. Supercontinent cycles, true polar wander, and very long-wavelength mantle convection. Earth and Planetary Science Letters 261, 551–564.
Zhong, S., Zuber, M.T., Moresi, L., Gurnis, M., 2000. Role of temperature-dependent viscosity and surface plates in spherical shell models of mantle convection. Journal of Geophysical Research: Solid Earth 105, 11063–11082.